JCI insight

RESEARCH ARTICLE

Tumor-infiltrating B cells signal functional humoral immune responses in breast cancer

Soizic Garaud,[1] Laurence Buisseret,[1] Cinzia Solinas,[1] Chunyan Gu-Trantien,[1] Alexandre de Wind,[2] Gert Van den Eynden,[3] Celine Naveaux,[1] Jean-Nicolas Lodewyckx,[1] Anaïs Boisson,[1] Hughes Duvillier,[1,4] Ligia Craciun,[2] Lieveke Ameye,[5] Isabelle Veys,[6] Marianne Paesmans,[5] Denis Larsimont,[2] Martine Piccart-Gebhart,[7] and Karen Willard-Gallo[1]

[1]Molecular Immunology Unit and [2]Department of Pathology, Institut Jules Bordet, Université Libre de Bruxelles, Brussels, Belgium. [3]Department of Pathology, GZA Ziekenhuizen, Sint-Augustinus campus, Wilrijk, Belgium. [4]Flow cytometry facility, [5]Data Centre, [6]Department of Surgery, and [7]Department of Medicine, Institut Jules Bordet, Université Libre de Bruxelles, Brussels, Belgium.

Tumor-infiltrating B cells (TIL-B) in breast cancer (BC) have previously been associated with improved clinical outcomes; however, their roles in tumor immunity are not currently well known. This study confirms and extends the correlation between higher TIL-B densities and positive outcomes through an analysis of HER2$^+$ and triple-negative BC patients from the BIG 02-98 clinical trial (10-year median follow-up). Fresh tissue analyses identify an increase in TIL-B density in untreated primary BC compared with normal breast tissues, which is associated with global, CD4$^+$, and CD8$^+$ tumor infiltrating lymphocytes (TIL); higher tumor grades; higher proliferation; and hormone receptor negativity. All B cell differentiation stages are detectable, but significant increases in memory TIL-B are consistently present. BC with higher infiltrates are specifically characterized by germinal center TIL-B, which in turn are correlated with T follicular helper (T_{FH}) TIL and antibody-secreting TIL-B principally located in tertiary lymphoid structures. Some TIL-B also interact directly with tumor cells. Functional analyses reveal that TIL-B are responsive to B cell receptor (BCR) stimulation ex vivo, express activation markers, and produce cytokines and Igs despite reduced expression of the antigen-presenting molecules HLA-DR and CD40. Overall, these data support the concept that ongoing humoral immune responses are generated by TIL-B and help to promote effective antitumor immunity at the tumor site.

Introduction

The key roles of the immune response in cancer progression have only recently come to the forefront, despite reports of immune cells infiltrating tumors that date to 1863 (1). Studies of human breast cancer (BC) show that tumor infiltrating lymphocytes (TIL) are more frequently observed in the triple-negative (TN) and HER2$^+$ subtypes. A TIL presence at diagnosis has been associated with improved disease-free survival (DFS) and overall survival (OS) after adjuvant chemotherapy and pathological complete responses to neoadjuvant therapy in both TN and HER2$^+$ BC (2–6).

Tumor infiltrates contain a heterogeneous population of immune cells frequently dominated by T cells but also containing B cells, NK cells, and myeloid-lineage cells including macrophages, mast cells, and neutrophils (7–9). Our laboratory used FACS to identify 3 TIL density groups by setting thresholds based on parallel analyses of normal breast tissues, finding differences among the lymphocyte subpopulations in these TIL density groups (10). Extensively infiltrated tumors (TIL^{hi} tumors) are distinguished by significantly higher tumor-infiltrating B cells (TIL-B) and CD4$^+$ TIL densities with a corresponding reduced frequency of CD8$^+$ TIL (10). T cell TIL have an activated phenotype characterized by CD69 and HLA-DR upregulation, constitutive expression of the costimulatory receptor CD28, and loss of naive T cell markers, including CD45RA and CCR7 (7). PD-1$^+$CD4$^+$ and PD-1$^+$CD8$^+$ T cell frequencies increase in BC compared with normal breast tissues, with up to 40% of the PD-1$^+$CD4$^+$ T cells characterized as CD4$^+$ T follicular helper (T_{FH}) cells located in tertiary lymphoid structures (TLS) (11, 12). Current data indicate that, in human BC, an

Authorship note: SG and LB contributed equally to this work.

Conflict of interest: The authors have declared that no conflict of interest exists.

Submitted: April 18, 2019
Accepted: August 8, 2019
Published: September 19, 2019.

Reference information: *JCI Insight*. 2019;4(18):e129641. https://doi.org/10.1172/jci.insight.129641.

important $CD4^+$ Th1 plus T_{FH} and $CD8^+$ TIL presence sustains antitumor immune responses while increasing balance in favor of $FOXP3^+$ Treg TIL is generally associated with worse clinical outcomes (11, 13–17). Although many experimental animal models and human studies have documented a key role for T cell TIL in antitumor immunity, relatively little is known about the role of TIL-B.

TIL-B have been identified in many tumor types, including high-grade serous ovarian cancer (HGSOC) (18), pancreatic adenocarcinoma (19), tongue squamous cell carcinoma (20), colorectal cancer (21), and cutaneous primary melanomas (22). They are principally enriched at the invasive margin, where they form dense aggregates opposite the tumor or are resident in TLS. A small fraction of TIL-B also sporadically infiltrates the peritumoral areas. TIL-B in TLS have been detected in 30% of melanomas and 8% of colorectal carcinoma, where they are correlated with earlier disease stages (21, 22). One BC study of TIL-B identified TLS in ~25% of tumors, where they incorporated up to 40% of total TIL (23). Our previous work found BC-associated TLS contain TIL-B and are detectable in 60% of all BC and 70% of TIL^+ BC (10). We further identified T cell TIL as principally memory T cells, while only 55% of TIL-B are memory B cells, although this is a significant increase over normal breast tissues (10). TLS have been reported to be prognostic for many types of cancer, including non–small cell lung cancer (NSCLC) (24, 25), colorectal cancer (26), renal cell carcinoma (27), melanoma (28), pancreatic cancer (29), and BC (11).

Early data from B cell–deficient mice suggested that TIL-B inhibit T cell–mediated regression of established tumors (30); however, in humans, it is now generally accepted that TIL-B signal a good prognosis for the majority of solid tumor types (31). High TIL-B have been associated with better survival in patients with cutaneous primary melanoma (22), colorectal carcinoma (21), tongue squamous cell carcinoma (20), HGSOC (18), NSCLC (32), and lower relapse rates in cervical cancer (33). Moreover, the prognostic significance of TIL-B and plasma cells (PC) was generally similar to that of $CD3^+$ and/or $CD8^+$ T cells and increased the prognostic effect of T cells (31). Interestingly, TIL-B resident in TLS were associated with better survival in pancreatic adenocarcinoma patients, but when randomly scattered in the tumor bed, they were not (19). Additionally, TIL-B resident in TLS were also correlated with higher $CD8^+$ TIL infiltration in these tumors.

In BC, a B cell metagene was shown to have prognostic value for high proliferative node-negative BC (34). Subsequently, a B cell/PC metagene exhibited a strong prognostic value in high proliferative estrogen receptor–positive (ER^+) BC, with lower prognostic value for ER^- BC and no prognostic value for low proliferative ER^+ BC (35). This was followed by an IHC study associating TIL-B with better survival in grade 3, ER^-, basal-like, and $HER2^+$ tumors (36). Denkert et al. demonstrated that 70% of LPBC are infiltrated with TIL-B and their presence is linked to pathological complete responses (2). Higher expression of B cell markers has also been correlated with a pathologic-complete response in TNBC patients treated with neoadjuvant chemotherapy (37). In contrast to invasive BC, higher numbers of TIL-B detected in preinvasive ductal carcinoma (pre-IDC) in situ were associated with shorter recurrence-free survival (38).

B cell immune functions extend well beyond being factories for antibody production to include cytokine production, antigen presentation, costimulation, and participation in the development of lymphoid tissue architecture. Conversely, B cells can perform immunosuppressive roles when differentiated to regulatory B cells (Breg) via their control of cellular immune responses. Prognostic and predictive values for TIL-B have also been reported in human cancer; however, their role is still controversial. TIL-B have been shown to mount tumor-specific autoantibody responses directed against tumor-associated antigens (TAA). Our recent work revealed that > 84% of the BC patients examined produce autoantibodies to 1 or more of the antigens present on a 91-TAA microarray (39). We further identified 8 antigens that elicit BC-associated autoantibody responses (39). In esophago-gastric adenocarcinoma, 48% of plasma samples were positive for 1 or more TAA (40). The ability of TIL-B to present antigen to $CD4^+$ TIL has also been demonstrated to function in NSCLC and alter the $CD4^+$ TIL phenotype (41). Direct tumor cell killing by TIL-B via antibody-independent mechanisms has also been reported (42). In hepatocellular carcinoma, margin-infiltrating B cells were found to mainly produce IFN-γ and IL-12p40 rather than IL-2, IL-4, IL-6, or IL-10 (43). The functionality of TIL-B in BC is currently unknown.

This study focuses on BC TIL-B because, in contrast to T cell TIL, their nature, phenotypic characteristics, and functional properties are not well characterized. Our data confirm and extend the correlation between TIL-B and improved clinical outcome in $HER2^+$ and TNBC. We show that TIL-B densities increase in all tumors compared with normal breast tissue. TIL-B are associated with global TIL ($CD45^+$), $CD4^+$ and $CD8^+$ TIL, higher tumor grade, and proliferation and hormone receptor negativity. Our data

demonstrate that highly infiltrated BC is distinguished by increased germinal center (GC) TIL-B, T_{FH} TIL, and antibody-secreting TIL-B, principally resident in TLS. Finally, our functional analyses show that TIL-B not only express activation markers, but they respond to B cell receptor (BCR) stimulation and produce B cell cytokines and Igs in situ.

Results

The prognostic value of TIL-B in HER2⁺ and TNBC. The long-term prognostic value of TIL-B was examined in node-positive HER2⁺ (n = 136) and TNBC (n = 113) BC patients from the BIG 02-98 phase III clinical trial (44). Enrollment accrued between 1998–2001 (prior to HER2⁺ BC patients receiving adjuvant trastuzumab), with a median follow-up of 10 years. Dual CD3/CD20 IHC staining performed on full-face tissue sections was independently scored for the percentage of global T cell TIL and TIL-B by 2 pathologists (45). Globally, TIL-B were associated with hormone receptor negativity and high histological grade and proliferation (Supplemental Table 1; supplemental material available online with this article; https://doi.org/10.1172/jci.insight.129641DS1). No significant associations were identified between TIL-B and age, surgery, histology, positive lymph nodes (LNs), tumor size, laterality, treatment, or radiotherapy. The median (50th percentile) IHC scores for TIL-B were 2.0% (interquartile range [IQR], 0.9%–4.5%) and 2.5% (IQR, 1.0%–6.25%) in the HER2⁺ and TNBC cohorts, respectively.

The optimal cut-off for TIL-B positivity in HER2⁺ tumors was 5.5%, which grouped 84% (n = 113) as TIL-B⁻ and 16% (n = 22) as TIL-B⁺. Events in the HER2⁺ cohort at 10 years were 58 (43%) for invasive DFS (iDFS) and 42 (31%) for OS. TNBC had an optimal cut-off at 2.75%, which categorized 51% (n = 58) as TIL-B⁻ and 49% (n = 55) as TIL-B⁺. The number of events in the TNBC cohort were 51 (35%) for iDFS and 40 (31%) for OS at 10 years. The Kaplan-Meier curves (Figure 1) show that a TIL-B presence is significantly associated with a better prognosis for both HER2⁺ and TNBC. In the HER2⁺ cohort, the 10-year iDFS for TIL-B⁺ was 80% vs. 52% for TIL-B⁻ (hazard ratio [HR], 0.34; 95%CI, 0.12–0.95, P = 0.03) and OS for TIL-B⁺ was 90% vs. 66% for TIL-B⁻ (HR, 0.25; 95%CI, 0.06–1.02, P = 0.04). In the TNBC cohort, the 10-year iDFS for TIL-B⁺ was 70% vs. 40% for TIL-B⁻ (HR, 0.40; 95%CI, 0.22–0.72, P = 0.002) and OS for TIL-B⁺ was 78% vs. 54% for TIL-B⁻ (HR, 0.44; 95%CI, 0.23–0.85, P = 0.01). We further found that iDFS and OS for both the HER2⁺ and TNBC cohorts plateaued before 5 years and was extended to 10 years, suggesting that the greatest impact of a TIL-B presence occurs in the first few years after diagnosis. Determination of the likelihood ratio (Supplemental Table 2) found that the addition of TIL-B (CD20) to T cell TIL (CD3) for HER2⁺ and, inversely, T cell TIL to TIL-B for TNBC added further prognostic information in multivariate analysis. Overall, these data confirm previous findings (46) and add new weight to the positive role of TIL-B, particularly when linked with T cell TIL, on long-term clinical outcomes.

B cells infiltrating normal and malignant breast tissues. B cells infiltrating fresh tissue specimens from normal (n = 62), nonadjacent nontumor (NANT; n = 312), benign tumor (n = 21), untreated IDC (n = 241), and untreated invasive lobular carcinoma (ILC; n = 62) were analyzed by FACS (Figure 2). The clinicopathological characteristics of the patients are detailed in Table 1, and the FACS gating strategies shown are in Supplemental Figure 1 (47). TIL-B were detected at significantly higher densities (absolute number/mg tissue) and percentages (percentage of total CD45⁺ cells) in invasive carcinomas (IDC and ILC) compared with normal breast tissues (Figure 2, A and B). B cell infiltration in NANT was similar to normal tissues. Alternatively, benign tumors contain significant increases in TIL-B density compared with normal and NANT tissues, although — as a percentage of total TIL — they are not markedly different. We also analyzed TIL-B as a function of disease stage. The accrual of TIL-B in IDC BC ends abruptly with stage IV tumors and local relapses, which are both poorly infiltrated and show no significant differences compared with normal tissues (Figure 2, C and D).

IDC and ILC patients were next grouped on the basis of TIL density (CD45⁺ TIL/mg) as previously defined: (a) TIL^{neg} with TIL densities equivalent to normal breast tissues, and TIL⁺ split into (b) TIL-intermediate (TIL^{int}), which falls between the normal tissue and NANT thresholds, and (c) TIL^{hi}, with densities above the NANT threshold (10). TIL-B increase significantly from TIL^{neg} to TIL^{int} to TIL^{hi} in IDC and TIL^{int} to TIL^{hi} in ILC compared with NANT, both as absolute numbers and as a percentage of CD45⁺ cells (Figure 2, E–H). Interestingly, only TIL-B densities, but not their percentage within the CD45⁺ cell compartment, increase significantly between the IDC TIL groups (Figure 2E). Thus, apart from a higher set point, TIL-B generally parallel global CD45⁺ TIL (Supplemental Table 3) with TIL^{hi} tumors characterized by their extensive presence.

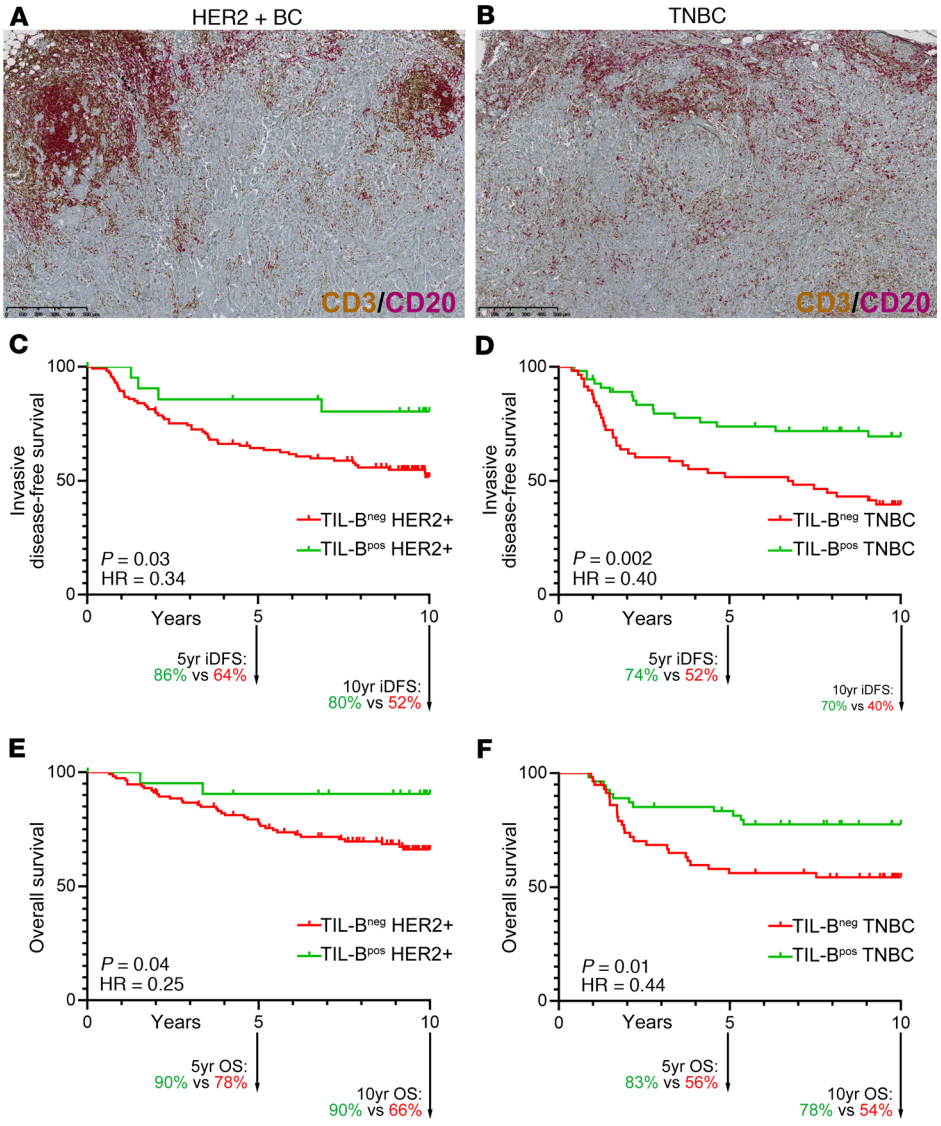

Figure 1. Prognostic value of tumor-infiltrating B cells in breast cancer. (**A** and **B**) Representative sections of HER2 (**A**) and TN (**B**) breast cancer with extensive TIL stained with CD3/CD20. (**C**–**F**) Kaplan-Meyer survival curves of 10-year invasive disease-free survival (iDFS) for 136 patients with HER2-positive disease (**C**), iDFS for 113 TN disease (**D**), overall survival (OS) for 136 patients with HER2-positive disease (**E**), and OS for 113 TN disease (**F**). Statistical analysis: log-rank (Mantel-Cox) test. See also Supplemental Tables 1 and 2.

FACS quantification of $CD4^+$ and $CD8^+$ TIL subpopulations in the same fresh BC specimens ($n = 311$) reveals that their presence is highly correlated with TIL-B (Supplemental Table 3). Because the majority of published studies identified TIL-B on IHC-stained tissues, we selected a subset of full-face blocks ($n = 25$) from our IDC BC cohort to comparatively score TIL on CD3/CD20 and CD4/CD8 dual IHC–stained tissues for comparison. The correlations between TIL-B quantified on paired data from $CD19^+$ TIL (FACS) and CD20 (IHC) were statistically significant (Supplemental Table 3). Once again, these data reveal that TIL-B are positively correlated with global, intrastromal, and intratumoral TIL; $CD3^+$ TIL; and the number of aggregates or TLS in the BC microenvironment. CD4 and CD8 scores from IHC-stained tissues were less well correlated, most likely due to some technical limitations with this stain. Clinicopathological parameters were correlated with TIL-B densities (determined by FACS) showing that high TIL-B densities are significantly associated with higher histological grade, higher tumor cell proliferation (Ki67), and hormone receptor negativity (Table 1). This is consistent with our previous observations for global $CD45^+$ TIL densities, with the exception of age (10). Overall, these data reveal higher infiltration of TIL-B in early BC in association with global TIL.

The immunophenotype of BC TIL-B. $CD19^+CD45^+$ B cells from peripheral blood mononuclear cells (PBMC), LNs, and breast tissues were FACS analyzed for the expression of various B cell differentiation and activation markers. CD38 and IgD, confirmed markers for defining naive to memory B cells, were used to identify and quantify B cell differentiation stages (Figure 3 and Supplemental Figure 2). The analysis of BC patient compared with healthy donor (HD) PBMC detected no significant differences

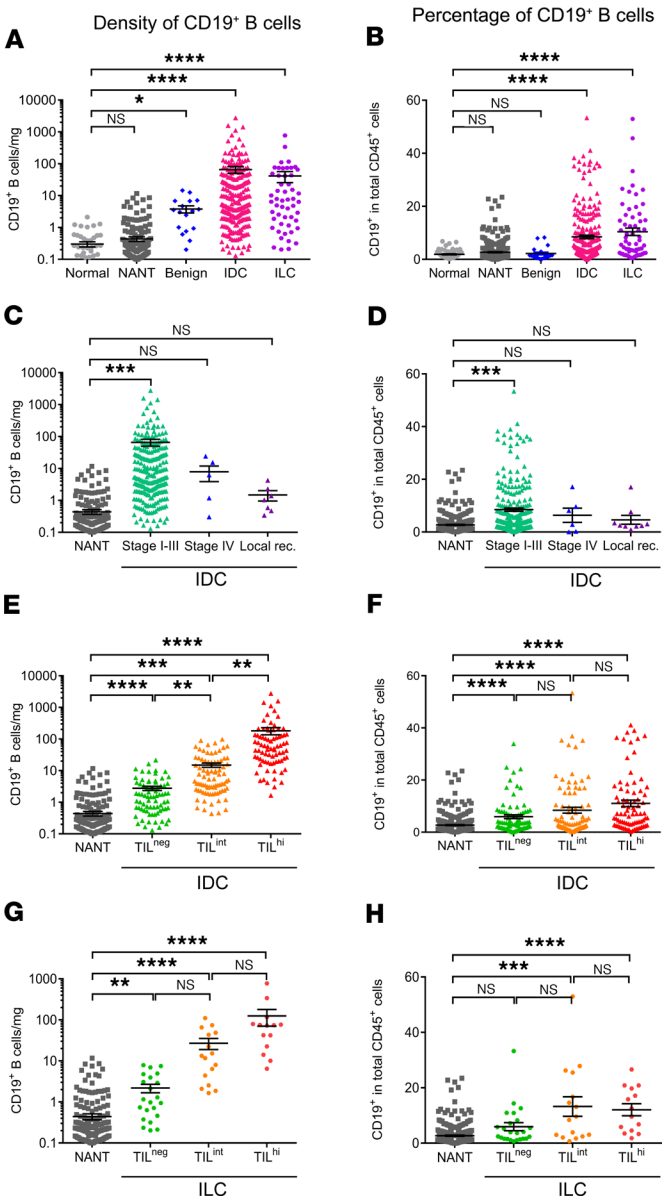

Figure 2. B cell infiltration in breast cancer tissues. (**A**–**H**) B cell infiltration was determined as an absolute number normalized to the weight (mg) of the tissue sample (**A**, **C**, **E**, and **G**) and as a percentage (**B**, **D**, **F**, and **H**) of CD45$^+$ TIL in the tissue by FACS. B cell infiltration was analyzed according to breast tissue type and cancer histology (**A** and **B**), BC stage (**C** and **D**), and global TIL infiltration in IDC (**E** and **F**) and in ILC (**G** and **H**). Data represent a combination of experiments involving individual patients and are displayed as the mean ± SEM by 1-way ANOVA with Dunn's multiple comparisons test (normal, n = 62; NANT, n = 312; benign, n = 21; IDC, n = 241; ILC, n = 62; stage I–III, n = 241; stage IV, n = 6, local recurrence (rec.), n = 9; IDC TIL^{neg}, n = 78; IDC TIL^{int}, n = 84; IDC TIL^{hi}, n = 79; ILC TIL^{neg}, n = 21; ILC TIL^{int}, n = 16; ILC TIL^{hi}, n = 14). *P < 0.05; **P < 0.01; ***P < 0.001; ****P < 0.0001. NANT, nonadjacent nontumor; IDC, invasive ductal carcinoma; ILC, invasive lobular carcinoma; TIL, tumor-infiltrating lymphocytes. See also Supplemental Table 3 and Supplemental Figure 1.

between any of the B cell subpopulations (Supplemental Figure 2A) and, therefore, functions as an internal baseline control for each patient. Involved LNs show a significant increase in early memory and memory TIL-B compared with reactive tonsils (Supplemental Figure 2B). In breast tissues, the frequency of naive B cells (within total CD19$^+$ B cells) was significantly reduced in parallel with an increase in memory B cells in benign, IDC, and ILC compared with normal breast tissue (Figure 3, A and B; B cell immunophenotypes in NANT tissues were not analyzed because of their low absolute numbers combined with limited tissue availability). Furthermore, the low TIL densities in stage IV IDC tissues were distinguished by a higher prevalence of memory TIL-B compared with IDC.

GC TIL-B significantly increase in TIL^{hi} compared with TIL^{neg} IDC, suggesting TLS are likely present in these highly infiltrated tumors (11, 12). Furthermore, GC TIL-B and T_{FH} TIL are consistently well correlated with one another (Figure 3, C and D, and Supplemental Table 4; T_{FH} TIL are identified as CD3$^+$CD4$^+$CD45$^+$CD200^{hi}PD-1^{hi} T cells because the canonical T_{FH} marker CXCR5 is downregulated on a significant number of these specialized TIL in BC; refs. 11, 12). GC TIL-B frequencies (centroblasts and centrocytes) are also positively correlated with PD-1$^+$CD4$^+$ and PD-1$^+$CD8$^+$ T cell TIL and antibody-secreting cells (ASC) but inversely correlated with memory TIL-B. Overall, these data characterize TIL^{hi} BC tissue as a receptive site for cooperative interactions between various active adaptive immune functions.

Table 1. TIL-B density association with clinicopathological parameters of the patients in our breast cancer cohort

	Number (%)	Median (Q1–Q3)	*P* value
Age (years)			
<50	74 (23.3)	11.14 (2.854–44.25)	0.4314
≥50	243 (76.7)	4.77 (1.488–34.07)	
Histology			
Ductal	241 (79.5)	6.06 (1.865–37.16)	0.7259
Lobular	54 (17.6)	6.44 (1.116–42.89)	
Mixed (ductal + lobular)	4 (1.3)	3.92 (0.9773–9.15)	
Other[A]	8 (2.6)	5.53 (0.7638–86.71)	
Node status			
Negative	154 (49.7)	6.12 (1.814–36.11)	0.2546
Positive	156 (50.3)	5.41 (1.492–36.82)	
Stage (AJCC staging)			
I	126 (44.4)	7.65 (1.94–39.49)	0.2583
II	116 (40.8)	5.02 (1.108–32.23)	
III	35 (12.3)	8.95 (2.299–48.85)	
IV	7 (2.5)	6.30 (0.3055–15.50)	
Histological grade			
1	62 (20.0)	4.91 (1.053–15.63)	**0.0023**
2	129 (41.6)	3.95 (1.326–19.71)	
3	119 (38.4)	16.63 (2.376–50.98)	
Ki67-proliferation index (IHC)			
<20%	173 (55.8)	3.91 (1.02–15.06)	**0.006**
≥20%	137 (44.2)	17.49 (2.36–54.58)	
Limphovascular embolism			
Absent	198 (65.1)	5.08 (1.478–39.33)	0.1559
Present	106 (34.9)	5.32 (2.023–26.47)	
Hormonal receptors (IHC)			
ER^-	49 (15.6)	34.07 (8.141–159.9)	**0.005**
ER^+	266 (84.4)	4.25 (1.329–22.75)	
PR^-	76 (24.2)	19.95 (3.086–94.27)	**0.0047**
PR^+	238 (75.8)	4.28 (1.473–22.5)	
HER-2 receptor (FISH)			
$HER\text{-}2^-$	263 (84.3)	5.16 (1.627–32.04)	0.3678
$HER\text{-}2^+$	49 (15.7)	8.95 (2.057–49.92)	
Size			
<20 mm	163 (51.7)	8.01 (2.057–43.04)	0.1301
≥20 mm	152 (48.3)	4.55 (1.04–25.44)	
Menopause			
Absent	92 (30.8)	10.59 (2.925–43.67)	0.7161
Present	207 (69.2)	4.29 (1.331–34.07)	

The *P* value was determined using the Wilcoxon rank or Kruskal-Wallis test when appropriate. Bold type indicates significant ($P < 0.05$). Q1 and Q3 represent the first and the third quartile, respectively. Data from flow cytometric analysis. [A]Other includes medullar, metaplastic, micropapillary, mucinous, and tubular BC. AJCC, American Joint Committee on Cancer staging.

Analysis of the late stages of TIL-B differentiation reveal that > 20% of $CD19^+$ TIL-B express surface IgG, in line with an affinity-matured response; however, significant differences between normal and tumor tissues were not detected (Supplemental Figure 2C). Tumor tissues also contain $CD5^+$ TIL-B (approximately 15% of TIL-B) but at lower frequencies than in normal tissues. ASC TIL-B, including $CD27^{hi}CD38^{hi}$ plasmablasts and PC, as well as $CD38^{hi}CD138^+$ PC, were identified but represent only minor TIL-B subpopulations. While no significant differences in ASC TIL-B were seen between normal and tumor tissues, a trend for more ASC in association with increased TIL infiltration was observed in IDC BC. These data show that humoral immune responses are generated at the tumor site, with GC TIL-B characteristic of more extensively infiltrated tumors and correlated with T_{FH} TIL, which are indicative of a TLS presence.

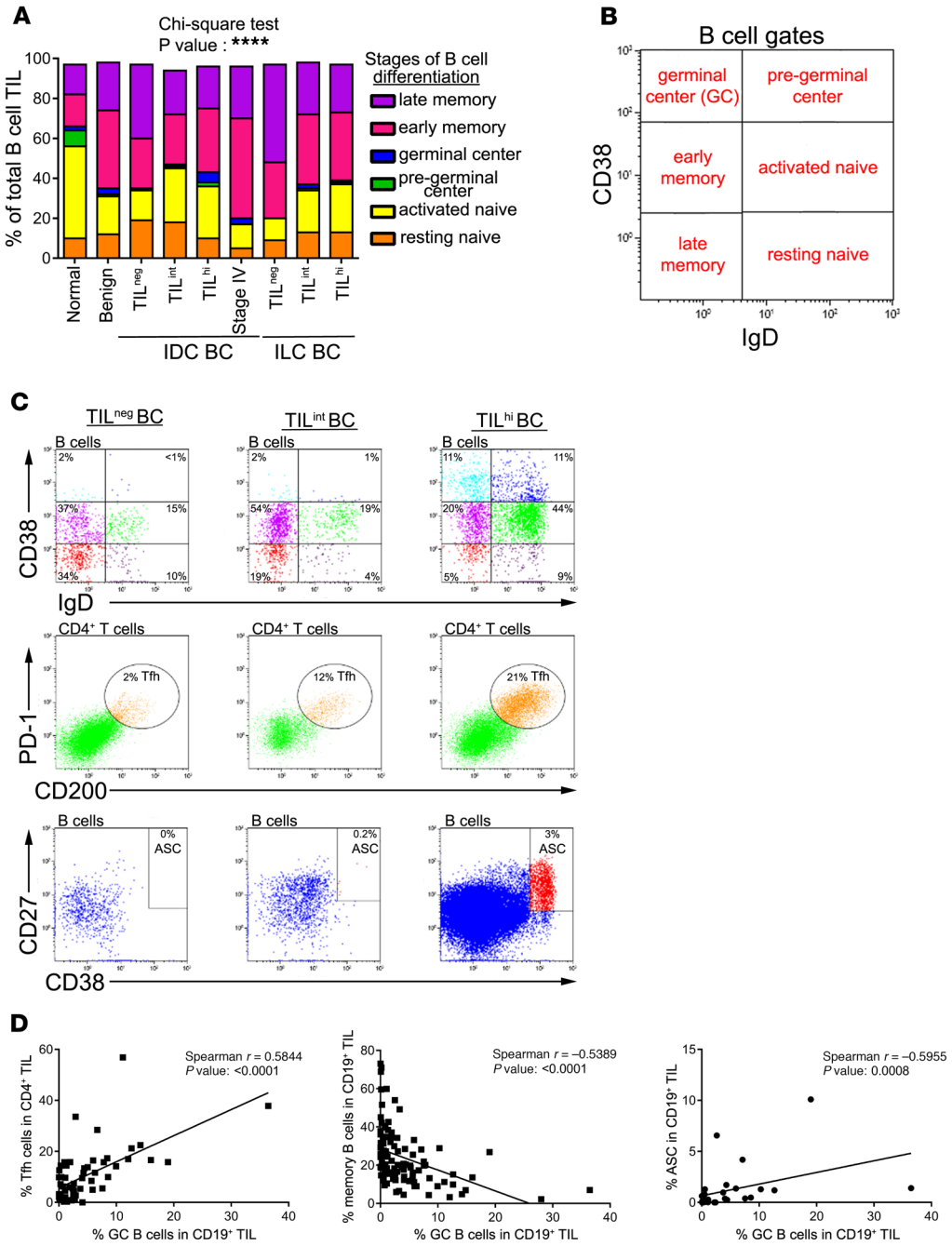

Figure 3. Phenotypic characterization of TIL-B in breast cancer tissues. (**A** and **B**) Stacked bars show the percentage of TIL-B subsets in total TIL-B according to the Bm classification (CD38 and IgD) (normal, n = 22; benign, n = 6; IDC TIL^{neg}, n = 9; IDC TIL^{int}, n = 27; IDC TIL^{hi}, n = 56; stage IV, n = 3; ILC TIL^{neg}, n = 4; ILC TIL^{int}, n = 10; ILC TIL^{hi}, n = 12). Data represent a combination of experiments involving individual patients and are displayed as the mean by χ^2 test. ****$P < 0.0001$. (**C**) Representative dot plots show percentages of Bm subsets, T_{FH}, and ASC in TIL^{neg}, TIL^{int}, and TIL^{hi} patients. (**D**) Graphs show the correlation between Bm3–4 and T_{FH} (n = 57), Bm5 (n = 101), and ASC (n = 28). Data represent a combination of experiments involving individual patients and are displayed as single value by Spearman test. Bm, mature B cells; T_{FH}, CD4$^+$ T follicular helper; ASC, antibody-secreting B cells; recurrence; TIL, tumor-infiltrating lymphocytes; IDC, invasive ductal carcinoma; ILC, invasive lobular carcinoma. See also Supplemental Figure 2 and Supplemental Table 4.

TIL-B composition, activation, and organization in BC. Our previous work determined that BC with extensive infiltrates are distinguished by both intratumoral and stromal TLS (11, 12, 48). This study focused on the spatial distribution and organization of TIL-B in TLS by analyzing BC (Figure 4) and tonsil (control; Supplemental Figure 3) formalin-fixed paraffin-embedded (FFPE) tissues. Immunofluorescence (IF) confocal microscopy

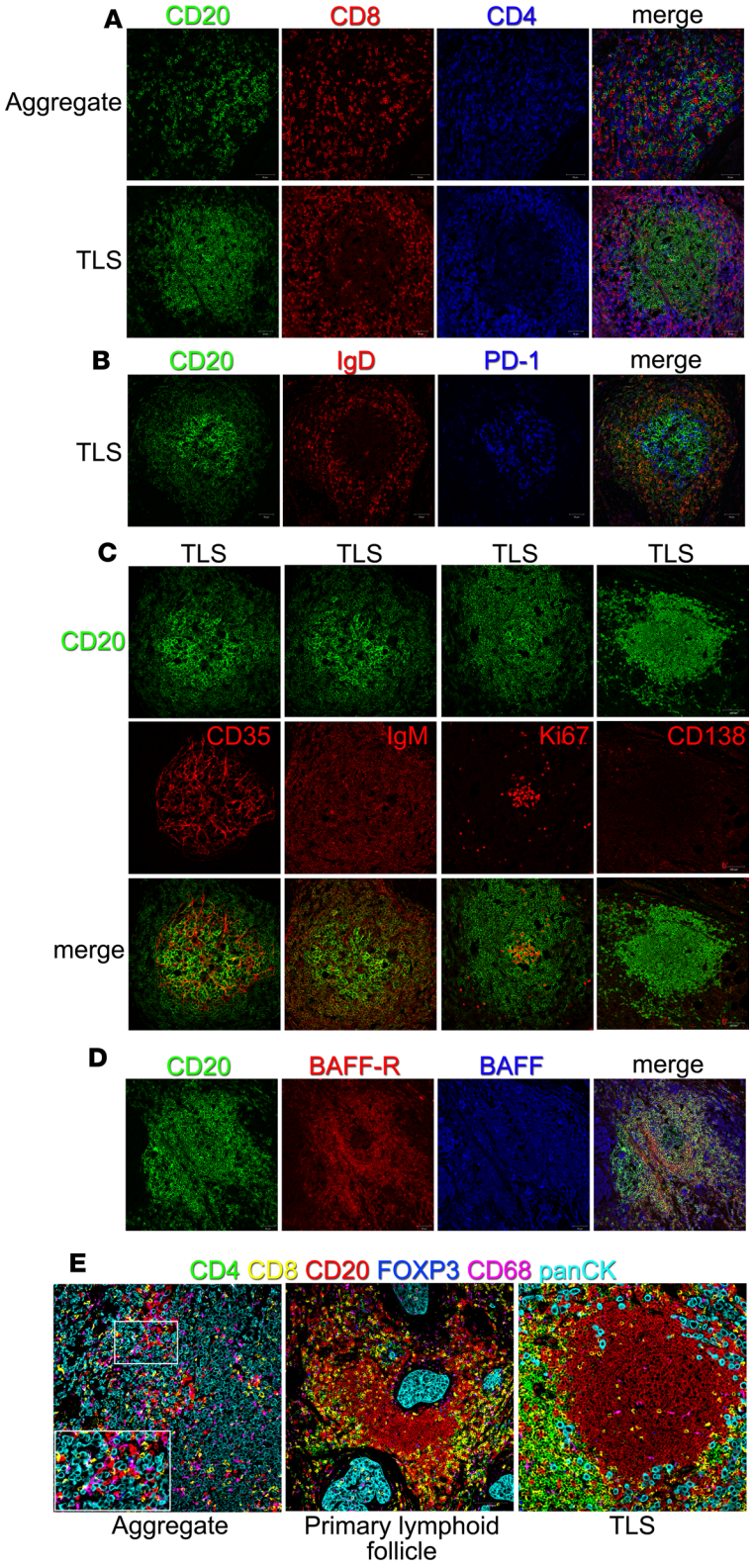

Figure 4. B cell organization in breast cancer tissues. (**A**–**D**) Immunofluorescent staining of tumor-associated aggregates and TLS on FFPE sections (20× magnification). Tumor-infiltrating lymphocytes were revealed by CD20 (green), CD8 (red), and CD4 (blue) (**A**). Germinal centers were identified by the absence of naive IgD$^+$ B cells (red) and the presence of PD-1$^+$ cells (blue) (**B**), as well as CD35$^+$ (red) follicular dendritic cells, IgM$^+$ (red) memory B cells, Ki67$^+$ (red) proliferating cells, and CD138$^+$ (red) plasma cells (**C**). BAFF (blue) and its receptor (red) were detected in germinal center of breast cancer (**D**). (**E**) Representative multiplexed IHC images of breast cancer. Tumor-infiltrating lymphocytes were revealed by CD20 (red), CD8 (yellow), CD4 (green), FOXP3 (blue), and CD68 (magenta) and tumor cells by panCK (cyan) (20× magnification). See also Supplemental Figure 3.

shows that TLS have a higher order organization that resembles secondary lymphoid organs (SLO), including a B cell follicle surrounded or adjacent to a T cell zone (Figure 4A and Supplemental Figure 3A). The T cell zone is principally composed of CD4$^+$ TIL with some CD8$^+$ TIL and IgD$^+$ follicular mantle TIL-B. T_{FH} cells, characterized as PD-1^{hi} cells, are detected in the light zone of tonsillar GC and in TLS (Figure 4B and Supplemental Figure 3A). In contrast, TIL aggregates are characterized by randomly distributed TIL-B, CD4$^+$, and CD8$^+$ T cell TIL (Figure 4A).

GC in SLO are key sites for generating humoral immune responses, which led us to use markers of active GC to determine whether TLS house similar activities. BC TLS are built on an interdigitating network of follicular DCs (CD35$^+$ FDC) similar to a tonsillar GC (Figure 4C and Supplemental Figure 3B). IgM$^+$CD20$^+$ TIL-B surround the GC with proliferating TIL-B (Ki67$^+$) at its center, again similar to tonsil tissue. CD138$^+$ PC are scarce and principally detected at the periphery of a BC TLS or tonsil GC, suggesting that, once matured, they quickly move into the periphery. B cell activation factor (BAFF; *TNFSF13B*) is a cytokine that potently activates B cells and together with its receptor (BAFF-R; *TNFRSF13C*) plays a role in B cell differentiation and survival (49–51). BAFF is ubiquitously expressed throughout BC TLS and tonsillar GC, while BAFF-R expression is restricted to the mantle zone in tonsillar GC with similar but less structured expression in BC TLS (Figure 4D and Supplemental Figure 3B).

An analysis of TIL-B interactions with other cells in the tumor microenvironment was accomplished using markers for subpopulations of T cell TIL (CD4, FOXP3, and CD8), TIL-B (CD20), macrophages (CD68), and tumor cells (panCK) in a multiplex IHC (mIHC) assay (Figure 4E, Supplemental Figure 3B, and Supplemental Figure 4). Interestingly, some TIL-B directly interact with tumor cells, as well as CD8$^+$ TIL and macrophages, both in aggregates, primary lymphoid follicles, and fully formed TLS. A region of BC aggregates was selected for analysis using the Phenoptr package of InForm software and identified 41% and 29% of TIL-B touching tumor cells and CD8-TIL, respectively (Supplemental Figure 4). These data show that specific TIL-B immunophenotypes are in contact with other immune cell subpopulations in BC-associated TLS and indicative of active humoral immune responses developing at the tumor site.

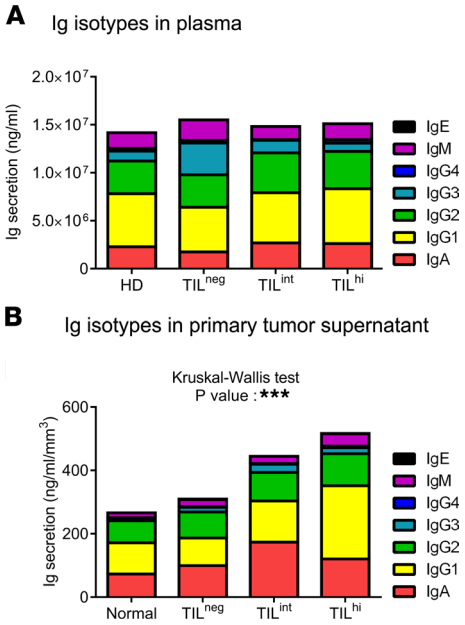

Figure 5. Ig repertoire in breast cancer. (**A** and **B**) Stacked bars quantify Ig subclasses in plasma from breast cancer patients and HD (**A**) and in breast tissue supernatant (**B**) (HD, n = 8; normal, n= 10; TIL^{neg}, n = 8; TIL^{int}, n = 4; TIL^{hi}, n = 9). Data represent a combination of experiments involving individual patients and are displayed as the mean ± SEM by 1-way ANOVA with Kruskal-Wallis test. ***P < 0.001. HD, healthy donors; TIL, tumor-infiltrating lymphocytes.

The functionality of TIL-B in BC. We evaluated the functional attributes of TIL-B, beginning with the balance of Ig isotypes present in fresh breast tissue supernatants (47) and plasma. Plasma from HD and BC patients, the latter stratified on TIL levels, were remarkably similar except for an increase in IgG3 detected in the TIL^{neg} group (Figure 5A). In the tissue supernatants, total Igs as well as the individual isotypes (including IgG subclasses) generally increase in parallel to the extent of immune infiltration from normal breast tissue to TIL^{hi} BC (Figure 5B). Statistically significant increases in IgG1, IgG2, IgG3, and IgM were detected between normal and malignant breast tissues, as well as in association with increasing TIL in BC. Interestingly, IgA was significantly increased in TIL^{int} compared with TIL^{neg} and TIL^{hi} BC, suggesting that the balance of isotypes may be influenced by immune activities associated with the level of infiltration in the tumor microenvironment.

B cells can also influence immune responses via soluble factors, with their subpopulations characterized by the cytokines they produce, similar to T cells. For example, effector B cells (Be1 and Be2) can prime naive CD4$^+$ Th1 or Th2 differentiation via their secretion of the canonical polarizing cytokines, IFN-γ, and IL-4, respectively (52). Cytokines, including IFN-γ, TNF-α, IL-1β, IL-4, IL-5, IL-6, IL-10, IL-13, IL-17A, IL-21, and IL-22, were analyzed in fresh breast tissue supernatants (mammary reductions, NANT, and tumors) together with plasma from HD and BC patients. In plasma, most of these cytokines were detectable (except for IL-1β, IL-2, and IL-5; data not shown) with elevated IFN-γ, TNF-α, IL-4, IL-13, and IL-17A and significant increases in IL-22 and IL-10 distinguishing BC patients from HD (Supplemental Figure 5A). Interestingly, a substantial increase in IL-6 was observed in plasma from TIL^{hi} BC compared with other BC patients and HD. Analysis of tissue supernatants again detected all of the cytokines tested (except for IL-17A; data not shown) in normal and abnormal breast tissues (Supplemental Figure 5B). The tissue milieus from normal breast, NANT, and BC are reflected in the composition of their supernatant, which generally followed a pattern of increased expression from normal to NANT, to BC. Statistically significant increases were found for TNF-β, IL-1β, IL-2, IL-13, and IL-22 in tumor relative to normal tissues. No significant differences were detected between normal breast and BC patient NANT tissues except for IL-10, which was expressed at very low levels but interestingly increased in both NANT and tumor relative to normal breast tissues.

The previous experiments clearly demonstrate that the BC tissue microenvironment is bathed in higher levels of many cytokines; however, our primary goal here was to identify those specifically produced by TIL-B. A comparative analysis of B cells sorted from tonsillar, LN, and BC tissues shows that TIL-B express a multitude of cytokines, except for IL-17A, IL-21, and IL-22, which are expressed minimally compared with B cells from tonsils and LNs (Figure 6). Interestingly, TIL-B express higher levels of type 1 cytokines (*IFNG* and *TNFA*) compared with B cells from secondary lymphoid tissues. Type 2 cytokines were more diverse with BC tissues characterized by higher *IL4*, equivalent *IL5*, and lower *IL6* and *IL13* expression levels. The immunosuppressive cytokines *IL10* and *TGFB* were also expressed by TIL-B, with *TGFB2* significantly increased

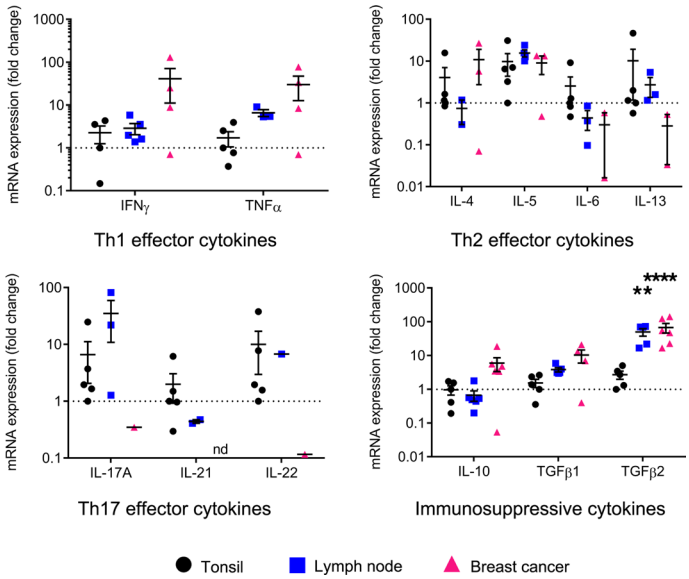

Figure 6. Cytokine profile of tumor-infiltrating B cells in breast cancer. Scatter plots show the transcript levels of cytokines in sorted B cells from lymph node (n = 6) and BC (n = 6), normalized to MLN51, and relative to B cells from tonsil (n = 5). Data represent a combination of experiments involving individual patients and are displayed as mean ± SEM by 1-way ANOVA with Tukey multiple comparisons test. $^{**}P < 0.01$; $^{****}P < 0.0001$. LN, lymph node; BC, breast cancer. See also Supplemental Figure 4.

compared with tonsillar B cells. These data suggest that TIL-B favor a type 1 cellular immune response and could thereby help to drive Th1 responses when present in the BC microenvironment.

While B cells are well known for their role as antibody producers, they also perform a variety of other immunological functions, including the induction of antigen-specific T cell activation via antigen presentation. The expression of costimulatory molecules such as CD40, CD80, and CD86 — together with HLA-DR, an antigen presenting cell/activation marker — were analyzed on PBMC, tonsillar B cells, and BC TIL-B (Figure 7A). HLA-DR and CD40 expression are significantly downregulated on TIL-B from IDC BC compared with PBMC B cells from HD and BC patients. A similar trend was also observed for TIL-B from ILC. Tonsillar B cells generally had low HLA-DR expression, while CD40 expression was comparable with PBMC. No significant differences were detected in the percentage of $CD80^+$ and $CD86^+$ TIL-B compared with PBMC or tonsillar B cells.

Decreased HLA-DR and CD40 expression could result from specific biological processes such as: (a) B cell differentiation to plasmablasts/PC, (b) the presence of exhausted tissue-like memory (TLM) B cells (recently described to have reduced CD40 expression; ref. 53), and/or (c) a tissue microenvironment favoring immunosuppression as described for BC DCs (54–56). Similar to previous findings (57), our study did not detect increases in plasmablasts or PC in tumor tissues compared with normal breast tissues and peripheral blood (Figure 7B). Furthermore, while TLM B cells ($CD19^+CD27^{lo}CD21^{lo}$) were detected in malignant breast tissues (Figure 7C), their frequency was only slightly increased in IDC and ILC BC compared with peripheral blood and tonsils, which was not statistically significant.

The functional consequences of the immunophenotypic changes we detected in HLA-DR and CD40 were evaluated by examining TIL-B intracellular calcium mobilization in response to stimulation with anti-BCR antibodies (ionomycin was used as a positive control; Figure 8). PBMCs and BC tissue homogenates (47) were rested overnight prior to loading Fluo-8, followed by FACS measurement of intracellular calcium levels in the $CD19^+$ B cell gate after the addition of BCR stimuli. TIL-B and HD B cells responded similarly with an immediate increase in intracellular calcium upon stimulation. This rapid increase of intracellular calcium suggests that the downregulation of HLA-DR and CD40 on TIL-B does not reflect an irreversible anergic state. Overall, these data show the functionality and multiple facets of TIL-B in antitumor immune responses — not only in the context of antibody production, but also Th1 responses and antigen presentation.

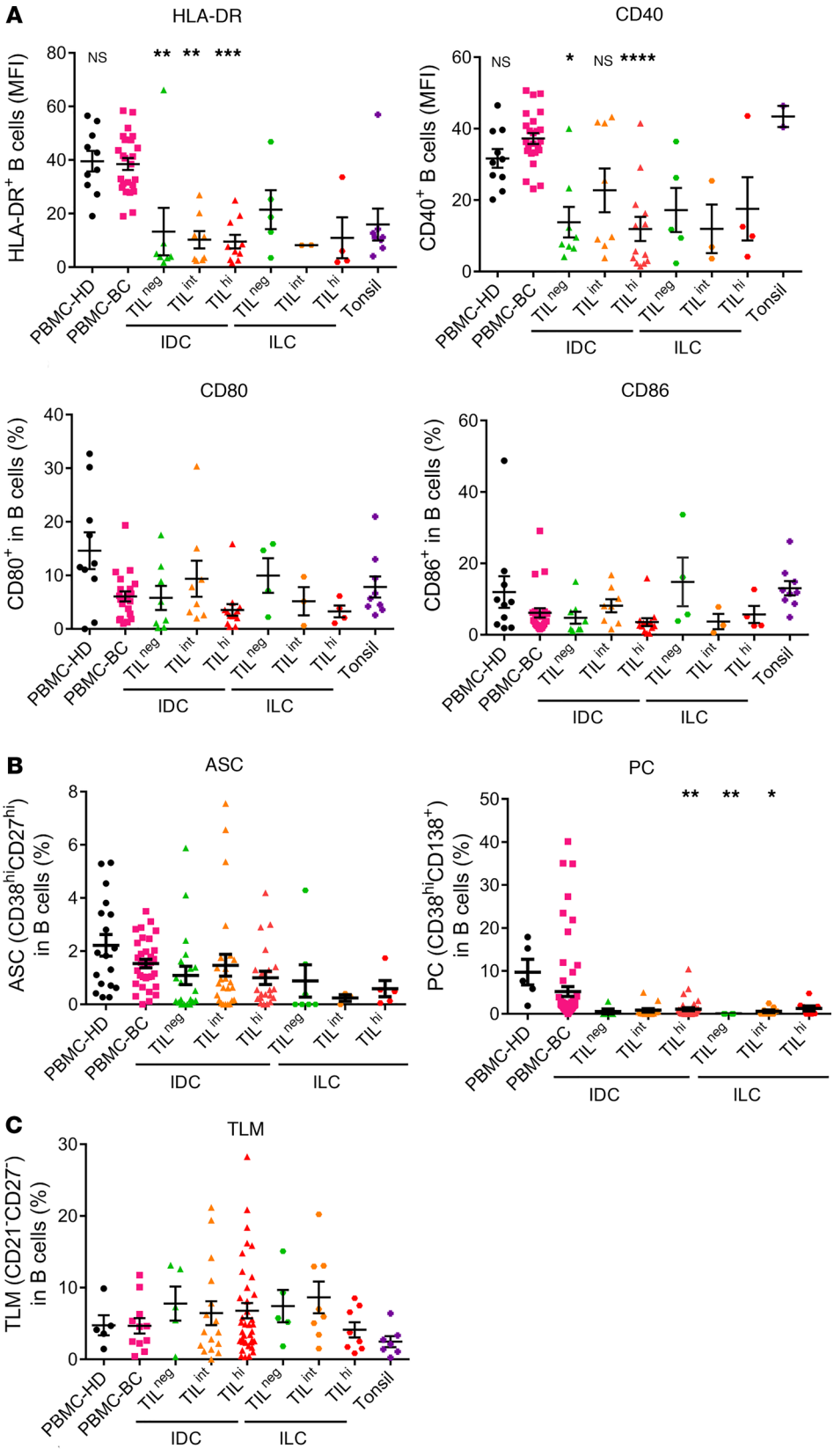

Figure 7. Antigen-presenting cells functions of B cells in breast cancer. (**A**) Scatter plots display the mean fluorescent intensity of HLA-DR and CD40, and the percentage of CD80 and CD86, on TIL-B (PBMC-HD, n = 10; PBMC-BC, n = 24; IDC TIL^{neg}, n = 8; IDC TIL^{int}, n = 8; IDC TIL^{hi}, n = 13; ILC TIL^{neg}, n = 5; ILC TIL^{int}, n = 3; ILC TIL^{hi}, n = 4; tonsil, n = 9). (**B**) Scatter plots display the percentage of ASC (PBMC-HD, n = 18; PBMC-BC, n = 33; IDC TIL^{neg}, n = 20; IDC TIL^{int}, n = 25; IDC TIL^{hi}, n = 21; ILC TIL^{neg}, n = 7; ILC TIL^{int}, n = 3; ILC TIL^{hi}, n = 5) and PC in B cells (PBMC-HD, n = 5; PBMC-BC, n = 63; IDC TIL^{neg}, n = 5; IDC TIL^{int}, n = 14; IDC TIL^{hi}, n = 36; ILC TIL^{neg}, n = 4; ILC TIL^{int}, n = 9; ILC TIL^{hi}, n = 8). (**C**) Scatter plot displays the percentage of tissue-like memory B cells using CD21$^-$CD27$^-$CD19$^+$ in B cells (PBMC-HD, n = 5; PBMC-BC, n = 11; IDC TIL^{neg}, n = 5; IDC TIL^{int}, n = 16; IDC TIL^{hi}, n = 37; ILC TIL^{neg}, n = 5; ILC TIL^{int}, n = 8; ILC TIL^{hi}, n = 8; tonsil, n = 7). Data represent a combination of experiments involving individual patients and are displayed as mean ± SEM by 1-way ANOVA with Dunn's multiple comparisons test. *P < 0.05; **P < 0.01; ***P < 0.001; ****P < 0.0001. PBMC, peripheral blood mononuclear cells; HD, healthy donors; BC, breast cancer; TIL, tumor-infiltrating lymphocytes; IDC, invasive ductal carcinoma; ILC, invasive lobular carcinoma; ASC, antibody-secreting cells; PC, plasma cells; TLM, tissue-like memory B cells.

Discussion

The data presented in this study show that TIL-B increase in invasive BC compared with normal breast tissues, which is particularly marked in TIL^{hi} tumors. TIL-B are significantly associated with T cell TIL, histological grade, proliferation (Ki67$^+$), and ER/PR status. While all B cell subsets are present, TIL^{hi} BC

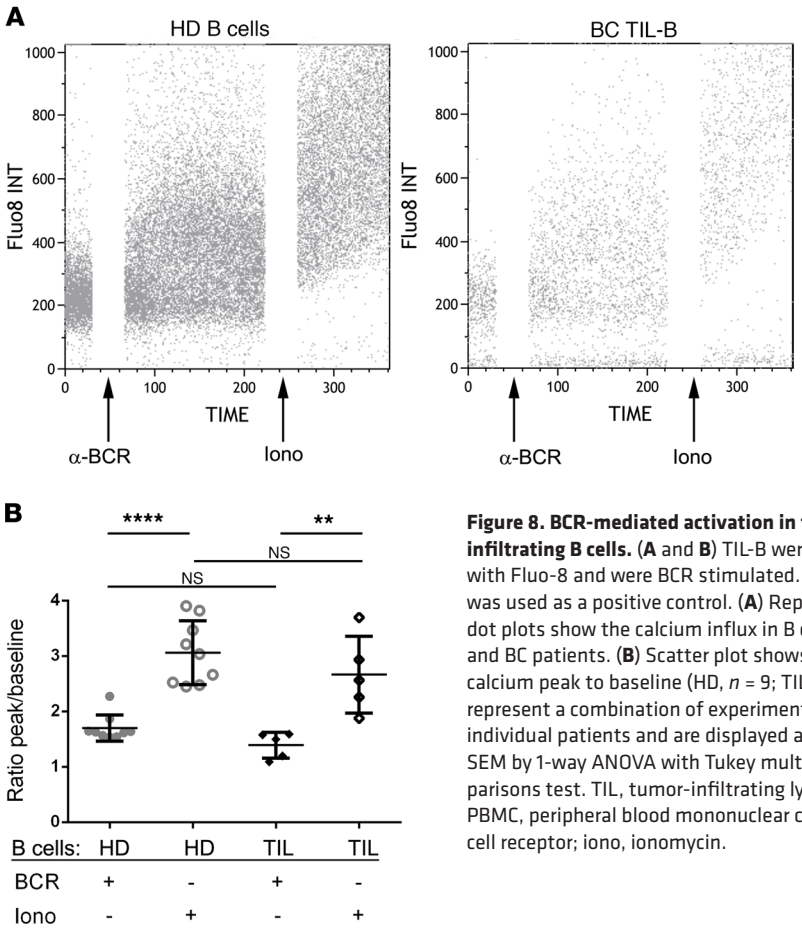

Figure 8. BCR-mediated activation in tumor-infiltrating B cells. (**A** and **B**) TIL-B were loaded with Fluo-8 and were BCR stimulated. Ionomycin was used as a positive control. (**A**) Representative dot plots show the calcium influx in B cells from HD and BC patients. (**B**) Scatter plot shows the ratio of calcium peak to baseline (HD, n = 9; TIL, n = 5). Data represent a combination of experiments involving individual patients and are displayed as mean ± SEM by 1-way ANOVA with Tukey multiple comparisons test. TIL, tumor-infiltrating lymphocytes; PBMC, peripheral blood mononuclear cells; BCR, B cell receptor; iono, ionomycin.

is specifically characterized by increased GC B cells in tight correlation with T_{FH} cells and ASC resident in TLS. These TIL-B are functionally responsive to antigen-receptor stimulation and produce cytokines and Igs despite their lower expression of APC markers. Overall, our data support the concept that ongoing humoral immune responses are associated with elevated and well-organized TIL, signaling that TIL-B play important roles in antitumor immunity.

Early studies variably associated the presence of TIL-B with either positive or negative clinical outcomes. More recently, Schmidt et al. reported that a B cell metagene had a positive prognostic value for metastasis-free survival in node-negative BC patients (n = 200; diagnosed between 1988–1998) (34). They further demonstrated that their B cell metagene provided independent prognostic information for high proliferative BC. Subsequently, Mahmoud et al. examined IHC-stained tissue microarrays from BC patients treated in the adjuvant setting (n = 1902; diagnosed between 1987–1998), finding that global TIL-B were associated with better long-term BC-specific survival, particularly in hormone receptor–negative, high-grade tumors (36). Interestingly, these data are also consistent with a human pancreatic adenocarcinoma study finding a correlation between a TIL-B/$CD8^+$ TIL presence and a more favorable prognosis in a tumor type that is generally lethal (19). In this study, we examined the impact of a TIL-B presence on the long-term survival of $HER2^+$ and TNBC patients diagnosed between 1998–2001 and treated in the adjuvant BIG 02-98 phase III clinical trial with a median follow-up of 10 years (45). TIL-B, scored on IHC-stained full-face sections, confirm the earlier gene expression and tumor tissue microarray data that global TIL-B density is associated with hormone receptor negativity, higher proliferation, higher histological grades, and higher stages. We further demonstrate that iDFS and OS in the uniformly treated TIL-B^+HER2^+ (without trastuzumab) and TNBC patients was remarkably high at 5 years, with OS remaining stable up to 10 years. Interestingly, we demonstrate added prognostic value for TIL-B plus T cell TIL in $HER2^+$ and for T cell TIL plus TIL-B in TNBC, which is consistent with preexisting adaptive immune responses in some patients (58). Overall, this study, together with previous studies, identifies TIL-B as an

important element of long-term BC survival; however, clinical outcome alone is not sufficient to establish a critical functional role for TIL-B in antitumor immunity.

Our earlier study of fresh breast tissues reported that immune infiltrates ($CD45^+$ TIL) in BC form a continuum from very low to exceedingly high immune activities at the tumor site (10). Further, we used normal breast tissues to set thresholds for stratifying TIL densities into TIL^{neg}, TIL^{int}, and TIL^{hi} BC. TIL^{hi} tumors contain significantly lower frequencies of $CD8^+$ TIL, offset by higher $CD4^+$ TIL and TIL-B. The present study, using our extended patient cohort, found that — similar to total $CD45^+$ TIL— TIL-B densities and frequencies increase continuously above the thresholds for normal breast tissue and TIL^{neg} (BC). We further observed that benign tumors (principally fibroadenomas) have an important TIL-B infiltrate. Miligy et al. reported that pure ductal carcinoma in situ (DCIS) tumors have higher numbers of TIL-B compared with DCIS associated with invasive BC (38). In their study, the TIL-B in pure DCIS were associated with larger tumor size, hormone receptor negativity, HER2 positivity, and a shorter recurrence-free interval. Together, these data support the concept that TIL-B may either actively contribute to BC development and/or attempt to help contain the developing malignancy.

TIL-B differentiation and maturation states have been studied in other human solid tumor types. NSCLC were found to contain all stages of B cell differentiation, although they were dominated by $IgD^-CD38^{+/-}$ memory B cells (25). The frequency of GC B cells was similar in blood, distant lung, and tumor tissues from individual patients, but generally, PC specifically increased in lung tumors compared with blood or LNs. We previously demonstrated that $CD19^+CD27^-$ naive B cells are the major subpopulation (65% of B cells) in normal breast tissues, with enrichment to a majority of $CD19^+CD27^+$ memory B cells (55% of TIL-B) in BC (10). In contrast to our BC data, no differences in B cell differentiation stages were detected between distant lung and NSCLC (25). We show here that ASC ($CD27^{hi}CD38^{hi}$) and PC ($CD38^{hi}CD138^+$) are minor subpopulations of BC TIL-B, with no significant differences observed between normal and tumor tissues. In contrast to NSCLC, our data parallel those from HGSOC, where a small population of IgD^-CD38^+ B cells, consistent with GC B cells, appear with an absence of $CD38^+CD138^+$ PC (57). This study also found that 80% of the ovarian tumors analyzed had small numbers of $CD38^+CD138^-$ plasmablasts. The data from breast and ovarian cancer suggest that, once matured, PC and ASC do not remain in normal or malignant breast tissues and, therefore, have likely moved to the periphery.

In addition to the increases in early and late memory B cells, we detected higher frequencies of GC TIL-B in association with T_{FH} cells and ASC in benign and invasive TIL^{hi} BC. Detailed characterization of TIL-B in 9 ovarian tumors found an overwhelming majority of $IgD^-CD38^{/lo}$ TIL-B, indicative of a memory B cell phenotype; however, these TIL-B were all $CD27^-$ (57). These atypical memory B cells have also been reported in ovarian metastases, in association with memory B cells with a more classical phenotype (59). In chronic infections characterized by an inability to eradicate the pathogen, B cells with an atypical memory phenotype have been shown to accumulate in patients (60). These data suggest that atypical memory TIL-B could be a subset of $CD27^-$ memory or TLM B cells arising in chronic inflammatory microenvironments. Tissue-resident memory T cells were initially described more than a decade ago in viral infection studies and are now viewed as the primary T cell subpopulation responsible for peripheral tissue surveillance and defense (61). Furthermore, these resident memory T cells not only serve in pathogen defenses, but have recently been shown to be functionally important in sustaining tumor dormancy by maintaining the equilibrium between malignant progression and immune surveillance (62). Similarly, TLM B cells were identified in virus studies, where they were described as having an exhausted phenotype in viremic HIV patient blood (63–65). TLM B cells express low levels of some distinguishing markers, exemplified by CD21 and CD27, but also high levels of inhibitory receptors, including Fc-receptor-like-4 (FCRL4), together with homing receptors specific for inflammatory sites. B cells with a TLM phenotype have been detected in tonsils, the blood of elderly individuals, and patients with microbial infections and autoimmune diseases (60). Bruno et al. recently identified $CD69^+HLA\text{-}DR^+CD27^-$ TIL-B in NSCLC, finding that they were associated with Treg TIL (41). In this study, we detected $CD21^{lo}CD27^{lo}$ TLM TIL-B in BC and positively correlated their presence with $PD\text{-}1^+CD4^+$ and $PD\text{-}1^+CD8^+$ TIL, both of which could be functionally exhausted TIL.

T cell or B cell exhaustion, distinct from anergy or senescence, is a reversible state of lymphocyte dysfunction characterized by deficient effector functions. Curtailing immune responses is an important regulatory mechanism for day-to-day immune activities; however, in situations of chronic antigen exposure, seen in autoimmunity, infection, and cancer, this often results in an inability to control disease. These dysfunctional T cells and B cells are greatly diminished in their response to antigen receptor stimulation, leading to decreased

proliferation, cytokine secretion, and/or antibody production (63, 66). In immune-responsive tumors, the accumulation of T cell TIL and TIL-B with a dysfunctional phenotype could reflect multiple rounds of antigenic-stimulation and efforts, albeit unsuccessful, to eradicate the tumor. Our previous study found that TIL-B are principally located in TLS (10), and while these structures may provide an order of protection from tumor-mediated suppression, they are also sites of chronic antigenic stimulation. Some of these tumors resemble an excluded phenotype, where TIL accumulate at the tumor bed border in aggregates or TLS. TLS^+ tumors have been shown to contain both active and inactive structures, suggesting that — in the chronic inflammatory tumor microenvironment — they may be driven from functional to nonfunctional over time (67, 68).

TLS formation and maintenance in tumors is just beginning to be understood, and the similarity of their composition and organization to SLO suggests that they potentially evolved via common mechanisms of lymphoid organogenesis. A variety of cell types, including lymphoid tissue–inducer cells, stromal cells, DCs, B cells, and T cell subpopulations, are critical partners in TLS formation. Cytokines and chemokines, including lymphotoxin A, CXCL13, CCL19, CCL21, IL-17, IL-22, and IL-23, have also been implicated in the initiation and organization of TLS (reviewed in ref. 69). Our laboratory recently demonstrated that the transcription factor FOXP1 is an important negative regulator of immune cell migration in BC via its impact on tumor cell cytokine and chemokine expression (70). Further, we found that CXCL13-producing T_{FH} (named $T_{FH}X13$) TIL promote local memory TIL-B differentiation and are potentially an early trigger of TLS formation in BC (12). The present study extends our observations on TLS formation by showing that mantle zone TIL-B express high levels of BAFF and its receptor, which reflects the pattern seen in SLO. This data is also consistent with a study demonstrating BAFF's critical role in the formation and compartmentalization of renal TLS (71). Our data suggest that CXCL13-producing T_{FH} cells guide TIL-B to inflammatory sites for TLS formation, where local concentrations of BAFF promote their survival, proliferation, and ultimate differentiation to memory cells, PC, or ASC.

The migration, differentiation, and maturation of TIL-B in tumor-associated TLS potentially drives the production of Igs that specifically recognize tumor antigens, thereby eliciting functional antitumor humoral immunity. This study examined Ig isotypes and IgG subclasses in plasma and primary tissue supernatants from normal and malignant breast tissues, finding that Ig concentrations were associated with TIL infiltration levels and characterized by a significant increase in IgG1 in TIL^{hi} BC. The link between polarization toward specific Igs and downstream effects on anti- or protumor immunity is currently unknown. In melanoma, polarization to IgG4 under Th2 inflammatory conditions was associated with poor clinical outcomes (72). This study found that melanoma antigen–specific IgG4 antibodies impaired the ability of the corresponding IgG1 to induce antibody-dependent tumor cell phagocytosis. Alternatively, anti-HER2 autoantibodies have been associated with a protective effect for primary or recurrent BC development (73). Thus, polarization of Ig isotypes and/or subclasses is likely to have a significant impact on tumor immunity.

TIL-B are functional, reflected by their production of autoantibodies specific for TAA, with a previous demonstration that BC TIL-B expand oligoclonally (74). Our recent analysis of paired primary tissue supernatant and plasma samples detected autoantibodies in > 84% of our BC cohort to 1 or more antigens on a 91-TAA microarray (39). The 3 most frequently recognized proteins were ankyrin repeat domain 30B like (ANKRD-30BL), COP9 signalosome subunit 4 (COPS4), and CTAG1B (also known as NY-ESO-1). This work also found that higher IgG but not IgA responses to BC-associated antigens were associated with shorter recurrence-free survival and lower $CD8^+$ TIL, suggesting that Ig isotypes may provide different biological functions in the tumor microenvironment (39). In the present study, global Ig production — and specifically IgG1 levels — increase in the tumor tissue supernatant as TIL levels graduate from low to intermediate to high, but this was also associated with a bump in IgA in the TIL^{int} group. Although there is no current precedent for interpreting these findings, a recent case report found an accumulation of PC and IgG in a metastatic LN from a lung cancer patient who achieved a partial response to immune checkpoint blockade (75). Alternatively, in primary melanoma, an increasing abundance of PCs predominantly producing IgG and IgA was associated with a worse prognosis (76). IgA production was further associated with melanoma progression, an effect that might be reflected in higher IgA in the TIL^{int} BC group. The importance of changing balances in Ig isotypes and IgG subclasses remains unknown; however, our data have identified a clear correlation between increased GC TIL-B and T_{FH} TIL, both expected to drive increased memory B cell and PC differentiation, leading to Ig production.

The versatility of B cells extends to their regulation of immune responses via cytokine production. Effector B cell subpopulations (Be1 and Be2), influenced by their surrounding milieu, produce distinct sets of cytokines (IFN-γ [Be1] or IL-4 [Be2]), which primes them to regulate naive $CD4^+$ T cell differentiation

and polarize them toward Th1 or Th2, respectively (52, 77). First described in hepatocellular carcinoma, margin-infiltrating effector TIL-B were found to principally produce IFN-γ and IL-12p40 but not IL-2, IL-4, IL-6, or IL-10 (43). We also primarily detected type 1 cytokines (IFN-γ and TNF-α) in BC TIL-B with significantly lower amounts of type 2 cytokines (IL-5, IL-6, and IL-13). These effector TIL-B, in association with $CD8^+$ T cells, were linked with improved survival both in hepatocellular carcinoma and ovarian cancer (57), suggesting that type 1 TIL-B may help to drive cytotoxic T cell responses. There is also accumulating evidence that TIL-B contain Breg, whose function is to regulate effector immune responses. Through their production of immunosuppressive cytokines, including IL-10 and TGF-β, the balance between effector TIL-B and Breg TIL-B could play an important role in suppressing antitumor immune responses. Consistent with previous studies in other human tumor types, we found that BC TIL-B can express IL-10 and TGF-β. Generally, these data support the notion that interactions between TIL-B and T cell TIL, particularly in the intimate microenvironment of a TLS, may be a driving force in activating and regulating humoral and cell-mediated antitumor immunity in human cancer.

B cells play important roles in immune responses that extend well beyond their canonical functions as antibody producers and include cytokine production, antigen presentation, costimulation, and contributions to lymphoid tissue development. Initial studies in B cell–deficient mice suggested that TIL-B generally inhibit T cell–mediated regression of established tumors (30); however, other murine tumor model studies found that TIL-B are necessary for optimal T cell activation and cellular immunity (78). These positive and negative effects on cellular immune responses directed by TIL-B could be due to differences in activation status, maturation stages, and B cell functions in different murine model systems. In this human study, we show that TIL-B express surface APC and costimulatory markers and are capable of responding to antigen engagement ex vivo. In ovarian cancer, TIL-B also express APC markers and were shown to colocalize with $CD8^+$ T cells, which suggests that they could be functioning as APC (57). This is supported by as recent NSCLC study demonstrating efficient antigen presentation to $CD4^+$ TIL by TIL-B (41). While most TIL-B express MHC class II (HLA-DR), 3 types of $CD4^+$ TIL responses to TIL-B have been identified: (a) activated where they spontaneously present endogenous tumor antigens to $CD4^+$ TIL; (b) antigen-associated, following restimulation with antigen; or (c) nonresponsive. Based on previously published work, together with the data presented here, we suggest that TIL-B can present antigen to $CD4^+$ TIL and thereby promote antitumor immune responses. Overall, this study shows that BC TIL-B are associated with an improved clinical prognosis and their presence primarily reflects an active, functional humoral immune response that likely transpires in BC-associated TLS.

Methods

Patient population and clinical samples. Fresh breast tissues, including tumor, normal tissue from mammary reduction, and NANT tissues, were obtained at the day of surgery from consenting BC patients diagnosed and treated at the Institut Jules Bordet between August 2012 and January 2016. The clinicopathological characteristics of BC patients are detailed in Table 1. Each fresh sample was measured and weighed, and an H&E stain was performed. Among a total number of 636 recruited tumors, only 56% were infiltrated with a sufficient number of B cells to perform ex vivo studies. Peripheral blood samples were obtained from 102 patients undergoing tumor resection for BC the day before the surgery. Peripheral blood samples from 23 healthy female adults were used as controls. Plasma were taken after centrifugation, clarified, and stored at –80°C.

For the retrospective study, TIL-B were assessed on samples from 136 patients with HER2 and 113 patients with TNBC included in the BIG 02-98 adjuvant phase III trial. TNBC subtype was defined as estrogen receptor–negative (ER^-), progesterone-negative (PR^-) and $HER2^-$ based on central IHC review that determined ER, PR, and HER2 status. HER2 subtype was defined as HER2 overexpression based on +3 by IHC or +2 by IHC and confirmed positive by fluorescent in situ hybridization. All samples were collected at baseline from the surgical specimen. Patient characteristics are detailed in ref. 45.

Tumor-infiltrated leukocytes and PBMC isolation. Dissected tumor fragments from fresh surgical specimens were directly transferred into 3 ml of X-VIVO 20 (Lonza). Tissue was manually minced before 2 rapid rounds of mechanical dissociation with the GentleMACS Dissociator (Myltenyi Biotec). The resulting cell suspension was filtered following each dissociator run using a 40-μm cell strainer (BD Falcon), washed with X-VIVO 20, centrifuged 15 minutes at 600 *g*, and resuspended in X-VIVO 20 before FACS analysis. The tumor supernatant was the initial 3ml of X-VIVO 20 recovered after the first round of dissociation, which was subsequently clarified by centrifugation for 15 minutes at 13,000 *g* (47).

PBMC were purified by density gradient centrifugation over Lymphoprep (Stemcell Technologies) and washed 3 times before FACS staining.

Flow cytometry and cell sorting. Cell suspensions were incubated with manufacturer-suggested dilutions of fluorescently labeled primary monoclonal antibodies (Supplemental Table 5) for 1 hour at 4°C in 100μl of X-VIVO 20, followed by washing with of PBS. After washing once, a lysing solution was used for the lysis of RBCs in cell suspension from breast tissues (VersaLyse, Beckman Coulter). Cells were then immediately acquired on a GALLIOS 10/3 cytometer and analyzed on Kaluza Flow Cytometry Analysis v1.2 software (Beckman Coulter).

Cell sorting was performed on breast tissue cell suspension using a Moflo ASTRIOS EQ 12/4 sorter (Beckman Coulter). B cells were sorted on a $CD3^{-}CD19^{+}$ lymphocyte gate. Cells were then lysed in TRIzol (Invitrogen) for RNA extraction and quantitative PCR (qPCR).

IHC staining and pathologic assessment. FFPE tissue sections (4 μm) were immunohistochemically stained for CD3/CD20 and CD4/CD8 dual staining on a Ventana Benchmark XT automated staining instrument (Ventana Medical Systems). A detailed protocol for the dual IHC stains is described in ref. 10. For CD3/CD20 dual staining, the slides were incubated with the ready-to-use polyclonal rabbit anti-CD3 primary antibody (IR50361-2, Agilent) and the ready-to-use mouse monoclonal anti-CD20 primary antibody (IR60461-2, Agilent). For CD4/CD8 dual staining, the slides were incubated with the ready-to-use monoclonal rabbit anti-CD4 primary antibody (BSB5150, BioSB) and the ready-to-use mouse monoclonal anti-CD8 primary antibody (IR62361-2, Agilent). Scoring TIL infiltration, lymphocyte subpopulation markers, and TLS on IHC-stained tissues was independently performed by 2 trained pathologists who were blinded to the clinical and experimental data.

IF microscopy. Sections (4-μm) of FFPE tissues were dewaxed twice in 100% xylene (VWR Chemicals) for 10 minutes, once in ethanol (Merck) 100%, once with 90% ethanol, once with 70% ethanol, and twice in H_2O for 5 minutes each baths. Then, slides were transferred in prewarmed sodium citrate buffer for antigen retrieval and incubated 30 minutes in the bath at 95°C, 20 minutes on the bench, and 5 minutes in running water. Tissues were blocked with IF buffer (PBS plus 1% BSA and 2% FBS) for 30 minutes at room temperature prior incubation of primary antibodies diluted in IF buffer overnight at 4°C. After 3 washes of 5 minutes in PBS, secondary antibodies diluted in IF buffer were incubated for 2 hours at room temperature. After washing, slides were mounted with ProLong Gold anti-fade mounting medium (Invitrogen) overnight and were visualized on a Zeiss LSM 710 confocal microscope equipped with a ×20/0.8 Plan-Apochromat dry objective (Carl Zeiss).

mIHC. FFPE tissue sections (4 μm) were processed manually for mIHC. Briefly, slides were heated at 37°C overnight and then deparaffinized and fixed in neutral-buffered 10% formalin. Slides were labeled for CD4 (Th cells), CD8 (cytotoxic T cells), CD20 (B cells), FOXP3 (Treg), CD68 (macrophages), pan-cytokeratin (cancer cells), and DAPI (all nuclei) using a serial same-species fluorescence-labeling approach that employs tyramide signal amplification and microwave-based antigen retrieval and antibody stripping according to the manufacturer's instructions (Opal 7 Solid Tumor Immunology kit, PerkinElmer). Slides were mounted with Vectashield Hardset Antifade Mounting Medium (VectorLaboratories). Samples were visualized on a Zeiss LSM 710 confocal microscope equipped with PMT spectral 34 canaux QUASAR (Carl Zeiss). Spatial interactions were performed using the Vectra Polaris imaging system (Akoya Biosciences). Multispectral images were analyzed with inForm Tissue Finder software (Akoya Biosciences) in order to segment tissue and cells, and phenotype cells. Spatial relationships between cellular phenotypes were determined using the phenoptrReports package (Akoya Biosciences).

qPCR. RNA was extracted using TRIzol Reagent (Invitrogen) and reverse transcribed into cDNA using High Capacity RNA-to-cDNA (Applied Biosystems) following standard procedures. qPCR reactions were performed using iTaq SYBR Green Supermix with ROX (Bio-Rad) on an ABI 7900HT Prism sequence detector (Applied Biosystems). The relative mRNA expression levels were calculated using the $2^{-\Delta\Delta ct}$ method.

Cytokines/Ig measurement by multiplex bead array. Soluble Igs and cytokines were determined by FACS using the multiple analyte detection system FlowCytomix (Bender MedSystems GmbH) performed according to the manufacturers' instructions. Plasma and tumor supernatant samples were clarified prior to use in the assay. The detection limits for IgG1, IgG2, IgG3, IgG4, IgA, IgM, IgE were 0.28, 1.15, 0.29, 1.20, 0.18, 10.17, and 0.02 ng/ml, respectively, and for IL-1β, IL-2, IL-4, IL-5, IL-6, IL-9, IL-10, IL-12p70, IL-13, IL-17A, IL-22, IFN-γ, and TNF-α were 4.2, 16.4, 20.8, 1.6, 1.2, 1.5, 1.9, 1.5, 4.5, 2.5, 43.3, 1.6, and 3.2 pg/ml. Quantification was done by FlowCytomix Pro Software (Bender MedSystems GmbH) and normalized to the tissue size (mm^3).

Flow cytometric analysis of calcium flux. PBMC and TIL were incubated overnight in RPMI 1640 media supplemented with 10% FBS, 2 mM glutamine, and antibiotics (50 μg/ml streptomycin and 50 U/ml penicillin) at 37°C and 5% CO_2. Cells were loaded with 5 μM Fluo-8 calcium indicator (Abcam) and 0.02% Pluronic

F-127 (Invitrogen); they were incubated at 37°C for 30 minutes and then at room temperature for another 30 minutes. Loaded cells were washed and subsequently stained with anti–CD4-APC (Miltenyi Biotec, 130-091-232, clone M-T466) and anti–CD19-APCVio770 (Miltenyi Biotec, 130-096-643, clone LT19) for 15 minutes at room temperature. Cells were washed and resuspended in HHBS buffer at 37°C for FACS analysis. After establishment of the baseline for 30 seconds, cells were stimulated with 50 μg/ml goat anti–human IgA+IgG+IgM (Jackson ImmunoResearch, 109-006-064, polyclonal), and the resulting calcium release was recorded for 150 seconds. A total of 2 μg/ml ionomycin (MilliporeSigma) served to elicit the maximum response over the last minute in all assays. The relative concentration of intracellular free calcium was measured as the median fluorescence ratio of the maximum peak poststimulation to baseline (79, 80).

Statistics. Unpaired data sets were compared by using the nonparametric 1-way ANOVA test (GraphPad Prism4 software). All values are expressed as mean ± SEM. In the BIG 02-98 series, we used the Mann-Whitney-Wilcoxon test and the χ^2 or Fisher exact test to assess differences in continuous and categorical variables, respectively. The association between 2 continuous variables was assessed with Spearman correlation, and the confidence intervals were calculated using Fisher Z-transformation. Survival curves were visualized using the Kaplan-Meier Method, and the logrank test was used to compare 2 survival curves. The HR with 95% CI was calculated using the Cox's proportional hazards model. The optimal cut-off of TIL-B in association to iDFS and OS was determined by the method of Contal and O'Quigley using the SASmacro %findcut (81), separately in the HER2$^+$ BC and TNBC groups. The outer 20% of the continuous variable distribution were excluded in this analysis to avoid having small numbers in one of the groups following dichotomization, in order to prevent substantial losses in statistical power. The considered cutoffs were from 0.50–9.00 with increases of 0.25 (e.g., 0.50, 0.75, 1.00, 1.25, 1.50, etc.). The added prognostic value of a variable was evaluated using the likelihood ratio test. All statistical analyses were performed 2 sided by using SAS 9.4 (SAS Institute Inc.). *P* values less than 0.05 were considered statistically significant (*$P < 0.05$; **$P < 0.01$; ***$P < 0.001$).

Study approval. All human specimens were acquired using a protocol approved by the Medical Ethics Committee of the Institut Jules Bordet with written informed consent obtained from each patient and donor prior to inclusion in the study (CE1981).

Author contributions

SG conceived the research and designed experiments with support from KWG. SG performed the majority of experiments with specialized help from LB, CS, CGT, CN, JNL, AB, and HD. LB and CS collected clinical case data. ADW and GVDE performed pathological evaluations. SG, LB, and KWG analyzed the data. SG, LB, CGT, and KWG discussed the data. SG and KWG interpreted the data. LC, GVDE, IV, and DL recruited and sampled patients. SG, LA, and MP performed statistical analyses. MPG proposed important concepts. KWG supervised the research. SG and KWG wrote and revised the manuscript, with all authors subsequently providing advice and approving the final manuscript.

Acknowledgments

The authors thank Gaelle Gillet and Naomi Faye Vermeulen for providing technical help, François Richard for providing insight on the statistical analyses, and the Center for Microscopy and Molecular Imaging (CMMI), which is supported by the Walloon Region and the ERDF (Wallonia-Biomed portfolio, 411132-957270). The BIG 02-98 study was supported with a grant from Sanofi. This work was supported by grants from the Fonds de la Recherche Scientifique – FNRS under grant T.0066.14, FNRS-Opération Télévie, Les Amis de l'Institut Bordet, Medic Foundation, Plan Cancer of Belgium, Fonds J.C. Heuson, and Fonds Lambeau-Marteaux. SG is a postdoctoral researcher of the FNRS-Operation Télévie.

Address correspondence to: Soizic Garaud, Molecular Immunology Unit, Institut Jules Bordet, Université Libre de Bruxelles, 127 Boulevard de Waterloo, B-1000 Brussels, Belgium. Phone: 32.2.541.7283; Email: soizic.garaud@bordet.be.

LB's present address is: Breast Cancer Translational Research Laboratory, Institut Jules Bordet, Université Libre de Bruxelles, Brussels, Belgium.

CG-T's present address is: Institut for Medical Immunology, Université Libre de Bruxelles, Gosselies, Belgium.

1. David H. Rudolf Virchow and modern aspects of tumor pathology. *Pathol Res Pract*. 1988;183(3):356–364.
2. Denkert C, et al. Tumor-associated lymphocytes as an independent predictor of response to neoadjuvant chemotherapy in breast cancer. *J Clin Oncol*. 2010;28(1):105–113.
3. West NR, Milne K, Truong PT, Macpherson N, Nelson BH, Watson PH. Tumor-infiltrating lymphocytes predict response to anthracycline-based chemotherapy in estrogen receptor-negative breast cancer. *Breast Cancer Res*. 2011;13(6):R126.
4. Loi S, et al. Prognostic and predictive value of tumor-infiltrating lymphocytes in a phase III randomized adjuvant breast cancer trial in node-positive breast cancer comparing the addition of docetaxel to doxorubicin with doxorubicin-based chemotherapy: BIG 02-98. *J Clin Oncol*. 2013;31(7):860–867.
5. Adams S, et al. Prognostic value of tumor-infiltrating lymphocytes in triple-negative breast cancers from two phase III randomized adjuvant breast cancer trials: ECOG 2197 and ECOG 1199. *J Clin Oncol*. 2014;32(27):2959–2966.
6. Loi S, et al. Tumor infiltrating lymphocytes are prognostic in triple negative breast cancer and predictive for trastuzumab benefit in early breast cancer: results from the FinHER trial. Ann Oncol. 2014;25(8):1544–1550.
7. Ruffell B, Au A, Rugo HS, Esserman LJ, Hwang ES, Coussens LM. Leukocyte composition of human breast cancer. *Proc Natl Acad Sci USA*. 2012;109(8):2796–2801.
8. Wong PY, Staren ED, Tereshkova N, Braun DP. Functional analysis of tumor-infiltrating leukocytes in breast cancer patients. *J Surg Res*. 1998;76(1):95–103.
9. Whitford P, Mallon EA, George WD, Campbell AM. Flow cytometric analysis of tumour infiltrating lymphocytes in breast cancer. *Br J Cancer*. 1990;62(6):971–975.
10. Buisseret L, et al. Tumor-infiltrating lymphocyte composition, organization and PD-1/ PD-L1 expression are linked in breast cancer. *Oncoimmunology*. 2017;6(1):e1257452.
11. Gu-Trantien C, et al. $CD4^+$ follicular helper T cell infiltration predicts breast cancer survival. *J Clin Invest*. 2013;123(7):2873–2892.
12. Gu-Trantien C, et al. CXCL13-producing TFH cells link immune suppression and adaptive memory in human breast cancer. *JCI Insight*. 2017;2(11):91487.
13. Seo AN, et al. Tumour-infiltrating CD8+ lymphocytes as an independent predictive factor for pathological complete response to primary systemic therapy in breast cancer. *Br J Cancer*. 2013;109(10):2705–2713.
14. Mahmoud SM, et al. Tumor-infiltrating CD8+ lymphocytes predict clinical outcome in breast cancer. *J Clin Oncol*. 2011;29(15):1949–1955.
15. Bates GJ, et al. Quantification of regulatory T cells enables the identification of high-risk breast cancer patients and those at risk of late relapse. *J Clin Oncol*. 2006;24(34):5373–5380.
16. Mahmoud SM, et al. An evaluation of the clinical significance of FOXP3+ infiltrating cells in human breast cancer. *Breast Cancer Res Treat*. 2011;127(1):99–108.
17. Liu S, et al. Prognostic significance of FOXP3+ tumor-infiltrating lymphocytes in breast cancer depends on estrogen receptor and human epidermal growth factor receptor-2 expression status and concurrent cytotoxic T-cell infiltration. *Breast Cancer Res*. 2014;16(5):432.
18. Milne K, et al. Systematic analysis of immune infiltrates in high-grade serous ovarian cancer reveals CD20, FoxP3 and TIA-1 as positive prognostic factors. *PLoS ONE*. 2009;4(7):e6412.
19. Castino GF, et al. Spatial distribution of B cells predicts prognosis in human pancreatic adenocarcinoma. *Oncoimmunology*. 2016;5(4):e1085147.
20. Lao XM, Liang YJ, Su YX, Zhang SE, Zhou XI, Liao GQ. Distribution and significance of interstitial fibrosis and stroma-infiltrating B cells in tongue squamous cell carcinoma. *Oncol Lett*. 2016;11(3):2027–2034.
21. Berntsson J, Nodin B, Eberhard J, Micke P, Jirström K. Prognostic impact of tumour-infiltrating B cells and plasma cells in colorectal cancer. *Int J Cancer*. 2016;139(5):1129–1139.
22. Garg K, et al. Tumor-associated B cells in cutaneous primary melanoma and improved clinical outcome. *Hum Pathol*. 2016;54:157–164.
23. Coronella-Wood JA, Hersh EM. Naturally occurring B-cell responses to breast cancer. *Cancer Immunol Immunother*. 2003;52(12):715–738.
24. Dieu-Nosjean MC, et al. Long-term survival for patients with non-small-cell lung cancer with intratumoral lymphoid structures. *J Clin Oncol*. 2008;26(27):4410–4417.
25. Germain C, et al. Presence of B cells in tertiary lymphoid structures is associated with a protective immunity in patients with lung cancer. *Am J Respir Crit Care Med*. 2014;189(7):832–844.
26. Remark R, et al. Characteristics and clinical impacts of the immune environments in colorectal and renal cell carcinoma lung metastases: influence of tumor origin. *Clin Cancer Res*. 2013;19(15):4079–4091.
27. Giraldo NA, et al. Orchestration and Prognostic Significance of Immune Checkpoints in the Microenvironment of Primary and Metastatic Renal Cell Cancer. *Clin Cancer Res*. 2015;21(13):3031–3040.
28. Ladányi A, et al. Density of DC-LAMP(+) mature dendritic cells in combination with activated T lymphocytes infiltrating primary cutaneous melanoma is a strong independent prognostic factor. *Cancer Immunol Immunother*. 2007;56(9):1459–1469.
29. Hiraoka N, Ino Y, Yamazaki-Itoh R, Kanai Y, Kosuge T, Shimada K. Intratumoral tertiary lymphoid organ is a favourable prognosticator in patients with pancreatic cancer. *Br J Cancer*. 2015;112(11):1782–1790.
30. Shah S, et al. Increased rejection of primary tumors in mice lacking B cells: inhibition of anti-tumor CTL and TH1 cytokine responses by B cells. *Int J Cancer*. 2005;117(4):574–586.
31. Wouters MCA, Nelson BH. Prognostic Significance of Tumor-Infiltrating B Cells and Plasma Cells in Human Cancer. *Clin Cancer Res*. 2018;24(24):6125–6135.
32. Al-Shibli KI, Donnem T, Al-Saad S, Persson M, Bremnes RM, Busund LT. Prognostic effect of epithelial and stromal lymphocyte infiltration in non-small cell lung cancer. *Clin Cancer Res*. 2008;14(16):5220–5227.
33. Nedergaard BS, Ladekarl M, Nyengaard JR, Nielsen K. A comparative study of the cellular immune response in patients with stage IB cervical squamous cell carcinoma. Low numbers of several immune cell subtypes are strongly associated with relapse of disease within 5 years. *Gynecol Oncol*. 2008;108(1):106–111.
34. Schmidt M, et al. The humoral immune system has a key prognostic impact in node-negative breast cancer. *Cancer Res*.

2008;68(13):5405–5413.
35. Bianchini G, et al. Molecular anatomy of breast cancer stroma and its prognostic value in estrogen receptor-positive and -negative cancers. *J Clin Oncol*. 2010;28(28):4316–4323.
36. Mahmoud SM, Lee AH, Paish EC, Macmillan RD, Ellis IO, Green AR. The prognostic significance of B lymphocytes in invasive carcinoma of the breast. *Breast Cancer Res Treat*. 2012;132(2):545–553.
37. Lee HJ, et al. Prognostic and predictive value of NanoString-based immune-related gene signatures in a neoadjuvant setting of triple-negative breast cancer: relationship to tumor-infiltrating lymphocytes. *Breast Cancer Res Treat*. 2015;151(3):619–627.
38. Miligy I, et al. Prognostic significance of tumour infiltrating B lymphocytes in breast ductal carcinoma in situ. *Histopathology*. 2017;71(2):258–268.
39. Garaud S, et al. Antigen Specificity and Clinical Significance of IgG and IgA Autoantibodies Produced *in situ* by Tumor-Infiltrating B Cells in Breast Cancer. *Front Immunol*. 2018;9:2660.
40. Schlößer HA, et al. B cells in esophago-gastric adenocarcinoma are highly differentiated, organize in tertiary lymphoid structures and produce tumor-specific antibodies. *Oncoimmunology*. 2019;8(1):e1512458.
41. Bruno TC, et al. Antigen-Presenting Intratumoral B Cells Affect $CD4^+$ TIL Phenotypes in Non-Small Cell Lung Cancer Patients. *Cancer Immunol Res*. 2017;5(10):898–907.
42. Kemp TJ, Moore JM, Griffith TS. Human B cells express functional TRAIL/Apo-2 ligand after CpG-containing oligodeoxynucleotide stimulation. *J Immunol*. 2004;173(2):892–899.
43. Shi JY, et al. Margin-infiltrating CD20(+) B cells display an atypical memory phenotype and correlate with favorable prognosis in hepatocellular carcinoma. *Clin Cancer Res*. 2013;19(21):5994–6005.
44. Francis P, et al. Adjuvant chemotherapy with sequential or concurrent anthracycline and docetaxel: Breast International Group 02-98 randomized trial. *J Natl Cancer Inst*. 2008;100(2):121–133.
45. Solinas C, etal. Immune parameters correlated with survival in triple negative and HER2-positive breast cancer patients with >10 years of follow-up. Paper presented at: 2018 San Antonio Breast Cancer Symposium; December 4–8, 2018; San Antonio, Texas, USA. http://cancerres.aacrjournals.org/content/79/4_Supplement/PD5-09. Accessed August 26, 2019.
46. Shen M, Wang J, Ren X. New Insights into Tumor-Infiltrating B Lymphocytes in Breast Cancer: Clinical Impacts and Regulatory Mechanisms. *Front Immunol*. 2018;9:470.
47. Garaud S, et al. A simple and rapid protocol to non-enzymatically dissociate fresh human tissues for the analysis of infiltrating lymphocytes. *J Vis Exp*. 2014(94):e52392.
48. Solinas C, et al. Immune Checkpoint Molecules on Tumor-Infiltrating Lymphocytes and Their Association with Tertiary Lymphoid Structures in Human Breast Cancer. *Front Immunol*. 2017;8:1412.
49. Batten M, et al. BAFF mediates survival of peripheral immature B lymphocytes. *J Exp Med*. 2000;192(10):1453–1466.
50. Mackay F, et al. Mice transgenic for BAFF develop lymphocytic disorders along with autoimmune manifestations. *J Exp Med*. 1999;190(11):1697–1710.
51. Pound J. A key role for BAFF in maintaining peripheral B cells. *Trends Immunol*. 2001;22(12):659.
52. Harris DP, et al. Reciprocal regulation of polarized cytokine production by effector B and T cells. *Nat Immunol*. 2000;1(6):475–482.
53. Li H, Borrego F, Nagata S, Tolnay M. Fc Receptor-like 5 Expression Distinguishes Two Distinct Subsets of Human Circulating Tissue-like Memory B Cells. *J Immunol*. 2016;196(10):4064–4074.
54. Pockaj BA, et al. Reduced T-cell and dendritic cell function is related to cyclooxygenase-2 overexpression and prostaglandin E2 secretion in patients with breast cancer. *Ann Surg Oncol*. 2004;11(3):328–339.
55. Pinzon-Charry A, et al. Numerical and functional defects of blood dendritic cells in early- and late-stage breast cancer. *Br J Cancer*. 2007;97(9):1251–1259.
56. Chen X, et al. CTLA-4 positive breast cancer cells suppress dendritic cells maturation and function. *Oncotarget*. 2017;8(8):13703–13715.
57. Nielsen JS, et al. CD20+ tumor-infiltrating lymphocytes have an atypical CD27- memory phenotype and together with CD8+ T cells promote favorable prognosis in ovarian cancer. *Clin Cancer Res*. 2012;18(12):3281–3292.
58. Disis ML, et al. Existent T-cell and antibody immunity to HER-2/neu protein in patients with breast cancer. *Cancer Res*. 1994;54(1):16–20.
59. Montfort A, et al. A Strong B-cell Response Is Part of the Immune Landscape in Human High-Grade Serous Ovarian Metastases. *Clin Cancer Res*. 2017;23(1):250–262.
60. Portugal S, Obeng-Adjei N, Moir S, Crompton PD, Pierce SK. Atypical memory B cells in human chronic infectious diseases: An interim report. *Cell Immunol*. 2017;321:18–25.
61. Shin H, Iwasaki A. Tissue-resident memory T cells. *Immunol Rev*. 2013;255(1):165–181.
62. Park SL, et al. Tissue-resident memory $CD8^+$ T cells promote melanoma-immune equilibrium in skin. *Nature*. 2019;565(7739):366–371.
63. Moir S, et al. Evidence for HIV-associated B cell exhaustion in a dysfunctional memory B cell compartment in HIV-infected viremic individuals. *J Exp Med*. 2008;205(8):1797–1805.
64. Zajac AJ, et al. Viral immune evasion due to persistence of activated T cells without effector function. *J Exp Med*. 1998;188(12):2205–2213.
65. Gallimore A, et al. Induction and exhaustion of lymphocytic choriomeningitis virus-specific cytotoxic T lymphocytes visualized using soluble tetrameric major histocompatibility complex class I-peptide complexes. *J Exp Med*. 1998;187(9):1383–1393.
66. Portugal S, et al. Malaria-associated atypical memory B cells exhibit markedly reduced B cell receptor signaling and effector function. *Elife*. 2015;4.
67. Siliņa K, Burkhardt C, Casanova R, Solterman A, van den Broek M. A Quantitative Pathology Approach to Analyze the Development of Human Cancer-Associated Tertiary Lymphoid Structures. *Methods Mol Biol*. 2018;1845:71–86.
68. Kather JN, et al. Topography of cancer-associated immune cells in human solid tumors. *Elife*. 2018;7:e36967.
69. Sautès-Fridman C, et al. Tertiary Lymphoid Structures in Cancers: Prognostic Value, Regulation, and Manipulation for Therapeutic Intervention. *Front Immunol*. 2016;7:407.
70. De Silva P, et al. FOXP1 negatively regulates tumor infiltrating lymphocyte migration in human breast cancer. *EBioMedicine*.

2019;39:226–238.
71. Kang S, Fedoriw Y, Brenneman EK, Truong YK, Kikly K, Vilen BJ. BAFF Induces Tertiary Lymphoid Structures and Positions T Cells within the Glomeruli during Lupus Nephritis. *J Immunol*. 2017;198(7):2602–2611.
72. Karagiannis P, et al. IgG4 subclass antibodies impair antitumor immunity in melanoma. *J Clin Invest*. 2013;123(4):1457–1474.
73. Tabuchi Y, et al. Protective effect of naturally occurring anti-HER2 autoantibodies on breast cancer. *Breast Cancer Res Treat*. 2016;157(1):55–63.
74. Coronella JA, et al. Antigen-driven oligoclonal expansion of tumor-infiltrating B cells in infiltrating ductal carcinoma of the breast. *J Immunol*. 2002;169(4):1829–1836.
75. Suyama T, et al. Successful treatment with nivolumab for lung cancer with low expression of PD-L1 and prominent tumor-infiltrating B cells and immunoglobulin G. *Thorac Cancer*. 2018;9(6):750–753.
76. Bosisio FM, et al. Plasma cells in primary melanoma. Prognostic significance and possible role of IgA. *Mod Pathol*. 2016;29(4):347–358.
77. Lund FE, Randall TD. Effector and regulatory B cells: modulators of CD4+ T cell immunity. *Nat Rev Immunol*. 2010;10(4):236–247.
78. DiLillo DJ, Yanaba K, Tedder TF. B cells are required for optimal CD4+ and CD8+ T cell tumor immunity: therapeutic B cell depletion enhances B16 melanoma growth in mice. *J Immunol*. 2010;184(7):4006–4016.
79. Schepers E, Glorieux G, Dhondt A, Leybaert L, Vanholder R. Flow cytometric calcium flux assay: evaluation of cytoplasmic calcium kinetics in whole blood leukocytes. *J Immunol Methods*. 2009;348(1-2):74–82.
80. Gergely L, Cook L, Agnello V. A simplified method for Ca2+ flux measurement on isolated human B cells that uses flow cytometry. *Clin Diagn Lab Immunol*. 1997;4(1):70–74.
81. Williams BA MJ, Mandrekar JS, Cha SS, Furth AF. *Technical Report Series #79: Finding Optimal Cutpoints for Continuous Covariates with Binary Time-to-Event Outcomes*. Rochester, Minnesota, USA: Mayo Clinic; 2006.